Dalton Transactions

Accepted Manuscript

ROYAL SOCIETY OF CHEMISTRY

www.rsc.org/dalton

Journal Name

ARTICLE

Uniform Fe_3O_4 coating on flower-like ZnO nanostructures by atomic layer deposition for electromagnetic wave absorption

Received 00th January 20xx,
Accepted 00th January 20xx

DOI: 10.1039/x0xx00000x

www.rsc.org/

Gengping Wan,[a] Guizhen Wang,*[a] Xianqin Huang,[a] Haonan Zhao,[a] Xinyue Li,[a] Kan Wang,[a] Lei Yu,[a] Xiange Peng[a] and Yong Qin*[b]

An elegant atomic layer deposition (ALD) method has been employed for controllable preparation of uniform Fe_3O_4-coated ZnO (ZnO@Fe_3O_4) core–shell flower–like nanostructure. The Fe_3O_4 coating thickness of the ZnO@Fe_3O_4 nanostructure can be tuned by varying the cycle numbers of ALD Fe_2O_3. When served as the additives for microwave absorption, the ZnO@Fe_3O_4–paraffin composites exhibit higher absorption capacity than the ZnO–paraffin composites. For ZnO@500-Fe_3O_4, the effective absorption bandwidth below –10 dB can reach 5.2 GHz and the RL values below –20 dB also cover a wide frequency range 11.6–14.2 GHz when the coating thickness is 2.3 mm, suggesting their potential application in treatment of the electromagnetic pollution problem. On the basis of experimental observations, a mechanism has been proposed to understand the enhanced microwave absorbing properties of the ZnO@Fe_3O_4 composites.

Introduction

Serious electromagnetic (EM) pollution problems from the extensive use of electronic equipment and wireless devices have called upon an urgent development of microwave absorption material (MAM).[1-8] Indeed, great advances have been achieved on model absorbers, and insights into the correlations of the materials morphology, size as well as chemical composition and absorption characteristics are crucial for not only understanding of EM wave absorbing mechanism, but also generating new concepts to guide the rational design of practical microwave absorbers.[9-14] Sun *et al.*[15] found that the absorption peaks could be controlled by varying the intersectional angles of aligned CNT films and the maximum reflection loss (RL) could be further increased by increasing the stacked number of aligned CNT films. Xia *et al.*[16] reported that hydrogenation successfully turned inactive TiO_2 into an excellent microwave absorber with an innovative collective-movement-of-interfacial dipole mechanism. Recently, it has also been confirmed that the integration of the dielectric–magnetic composition and unique morphology into the unique core-shell structure is an effective strategy to acquire high-performance microwave absorbers due to intensified polarization at interfaces and its associated relaxation loss, which provides an elegant method for MAM innovations and inspires further developments of other exciting MAMs.[17-23] For example, Yuan *et al.*[24] fabricated novel 3-D ordered arrays of core–shell microspheres consisting of Fe_3O_4 cores and ordered mesoporous carbon shells, which showed excellent microwave absorption performances with maximum RL of up to −57 dB at 8 GHz, and large absorption bandwidth (7.3–13.7 GHz, < −10 dB). Yu *et al.*[25] found that FeCo nanoparticle embedded nanoporous carbon composites exhibited a maximum RL of −21.7 dB at a thickness of 1.2 mm.

ZnO has been widely investigated as a major annexing agent of microwave absorbers due to its low cost, non-toxic nature, long-term stability, semiconductive, and piezoelectric features.[26-29] A core problem in exploiting new types of functional ZnO absorption materials is how to enhance their EM wave absorbing efficiency. Many studies demonstrated that modifying ZnO could improve its absorption properties by controlling its structure, compositing with other materials or introducing other constituents into the lattice.[30-33] For example, Wang *et al.*[34] prepared ZnO/PVDF composites via a simple hot-press method and found that the RL of the composite with a filler content of 10 wt% had two peaks that could reach −15.90 dB at 6.60 GHz and −25.44 dB at 16.48 GHz. The mechanism for the increase in absorption properties could be explained by the Debye relaxation theory. Lu *et al.*[35] reported the synthesis of multi-wall carbon nanotubes decorated with ZnO nanocrystals by a mild solution-process and investigated its high temperature microwave absorption properties. Their results showed that the absorbing frequency of the composites almost covers the full X-band for RL ≤ −10 dB. Despite these great developments in the synthesis of ZnO based MAMs, the facile synthesis of ZnO composites with well-defined core–shell structure including the coating thickness and uniformity remains a challenge.

Herein, we synthesized the interesting Fe_3O_4-coated ZnO (ZnO@Fe_3O_4) core–shell composite materials by an atomic layer deposition (ALD) technology and investigated the dielectric and microwave absorption properties of composites. The results show that ZnO@Fe_3O_4 is an excellent MAM candidate benefiting from the

[a] Key Laboratory of Tropical Biological Resources of Ministry of Education, Hainan University, Haikou 570228, China E-mail: wangguizhen0@hotmail.com
[b] State Key Laboratory of Coal Conversion, Institute of Coal Chemistry, Chinese Academy of Sciences, Taiyuan 030001, China.
Electronic Supplementary Information (ESI) available: [EDS, dielectric loss tangent and Cole-Cole semicircle]. See DOI: 10.1039/x0xx00000x

uniform core-shell structure which induces the intensified interfacial polarization enlarged microwave absorption.

Experimetal

Preparation of ZnO. The ZnO used in this work was synthesized by a hydrothermal method as reported previously.[32] Typically, 40 mL of 20 mmol·L^{-1} zinc acetate aqueous solution was mixed with a NaOH aqueous solution (0.3 mol·L^{-1}) of the same volume under vigorous magnetic stirring at room temperature. The mixture solution was then transferred into a 100 mL Teflon-lined stainless steel autoclave and was kept at 160 °C for 5 h. The resultant white solid product was centrifuged, washed with distilled water, and dried at 45 °C in a vacuum.

Synthesis of ZnO@Fe_3O_4. The ALD process was carried out in a home-made, closed type, hot-wall ALD reactor. Prior to ALD, the ZnO was dispersed in ethanol by ultrasonic agitation and then dropped onto a quartz wafer. After being air-dried, the Fe_2O_3 coatings were deposited by sequential exposure of the ZnO to Ferrocene ($FeCp_2$) and O_3. The temperature of $FeCp_2$ precursor was maintained at 100 °C and the deposition was conducted with a substrate temperature of 250 °C. Finally, after the ALD process, the sample was transferred to a furnace and reduced at 450 °C in 5% H_2/Ar atmosphere for 2 h. The sample was collected and was denoted as ZnO@n-Fe_2O_3 or ZnO@n-Fe_3O_4, where n means the cycle number of the Fe_2O_3 ALD.

Sample characterization. X-ray diffraction (XRD) patterns were collected on a Bruker D8 Advance X-ray diffractometer using a Cu *Kα* source (*λ* = 0.154056 nm). Scanning electron microscopy (SEM) images were obtained using a HITACHI S-3000N microscope. Transmission electron microscopy (TEM) and high-resolution TEM (HRTEM) images were taken on a JEOL-2100 microscope instrument at an acceleration voltage of 200 kV. The composition and elemental maps of the samples were analyzed by energy-dispersive X-ray (EDX) spectroscopy using an EDX attachment to the SEM instrument. Raman spectroscopy was performed on a Renishaw inVia Reflex Raman microscope using 532 nm green laser excitation. The chemical compositions of the samples were determined by atomic absorption spectroscopy (AAS, TAS-990 Super AFG). The specimens for measuring the EM properties were prepared by uniformly mixing 60 wt% ZnO or ZnO@Fe_3O_4 with paraffin and pressing the mixture into a cylindrical shape. Then the cylinder was cut into a toroid of 7.00 mm outer diameter and 3.04 mm inner diameter for measurement. The relative permeability and permittivity values of the mixture were determined and obtained by measuring the S_{11} and S_{21} parameters between 2 and 18 GHz with an AV3629D network analyzer by using the transmission/reflection coaxial line method.

Results and discussion

The morphologies and microstructures of the starting ZnO used in this study were characterized by using SEM (Fig. 1a) and TEM (Fig. 1b). It can be seen that ZnO presents a flower-like hierarchical structure assembled by the ZnO nanorods with a diameter of 100–400 nm and a length of up to a few microns. The HRTEM image (Fig. 1c) and FFT diffraction pattern (inset to Fig .1c) confirm that the flower-like ZnO is the hexagonal phase of zincite. The well-defined crystalline lattice spacing of 0.19 and 0.28 nm can be indexed as (102) and (100) crystal planes of ZnO, respectively.

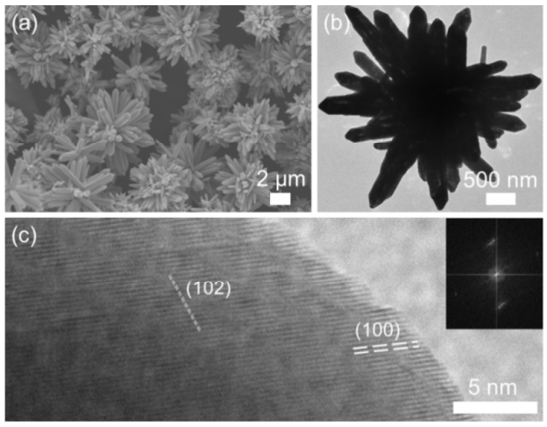

Fig. 1 (a) SEM, (b) TEM and HRTEM images of ZnO.

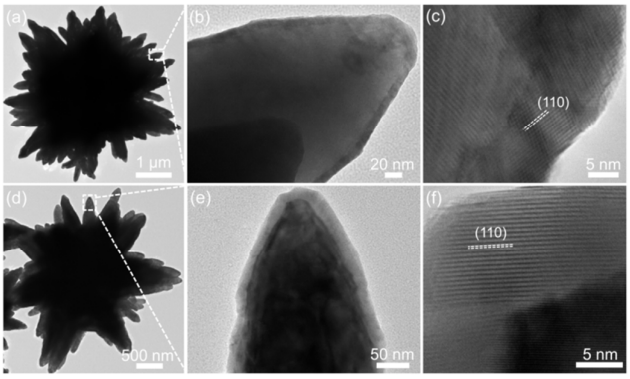

Fig. 2 TEM and HRTEM images of (a)–(c) ZnO@500-Fe_2O_3 and (d)–(f) ZnO@1000-Fe_2O_3.

Fig. 2a and b show low-magnification TEM images of ZnO@Fe_2O_3 obtained by applying 500 ALD cycles of Fe_2O_3 deposition. It is clearly seen that the surface of ZnO nanorod is covered with a very uniform Fe_2O_3 shell with a thickness of about 10 nm. The HRTEM image shows the well-defined crystalline lattice spacing of 0.25 nm, corresponding to the (110) crystal plane of rhombohedral phase Fe_2O_3 (Fig. 2c). The thickness of Fe_2O_3 coating can be easily tuned by adjusting the cycle numbers of the Fe_2O_3 ALD process. Fig. 2d and e show TEM images of the product after 1000 Fe_2O_3 ALD cycles. The formed ZnO@Fe_2O_3 core-shell structures are clearly visible due to their different contrasts. The thickness of Fe_2O_3 shells increases with the increase of ALD cycles and amounts to about 20 nm, which corresponds to a growth rate of about 0.2 Å per cycle. The lattice fringes from HRTEM images (Fig. 2f) also reveal the features of rhombohedral phase Fe_2O_3.

The flower-like ZnO@Fe_3O_4 core-shell structures can be readily obtained by annealing ZnO@Fe_2O_3 at 450 °C for 2 h under a mixture

of Ar/H_2 flow in a tube furnace. After a reduction process, the colour of products changed from yellow to black. As shown in Fig. 3a and b and Fig. 3d and e, it can be seen that the ZnO@Fe_3O_4 core-shell nanostructures have similar morphology and size with the ZnO@Fe_2O_3. In comparison to ZnO@Fe_2O_3, the average thicknesses of Fe_3O_4 shells measured by TEM images are also about 10 and 20 nm for the ZnO@500-Fe_3O_4 and ZnO@1000-Fe_3O_4, respectively. The negligible variation in shell thickness should be ascribed to that only approximately 3.33 wt% shrinkage was produced from the release of oxygen anions in the reduction treatment (from Fe_2O_3 to Fe_3O_4). The well-defined crystalline lattice spacing of 0.30 and 0.49 nm are observed, corresponding to the (220) and (111) crystal planes of Fe_3O_4 (Fig. 3c and f), respectively. The energy dispersive X-ray spectroscopy (EDS) elemental maps of Zn, O and Fe demonstrate that the Fe element is equally distributed on the surface of ZnO and maintains a consistent flower-like morphology, which furthermore indicates the perfect core–shell configuration (Fig. 4).

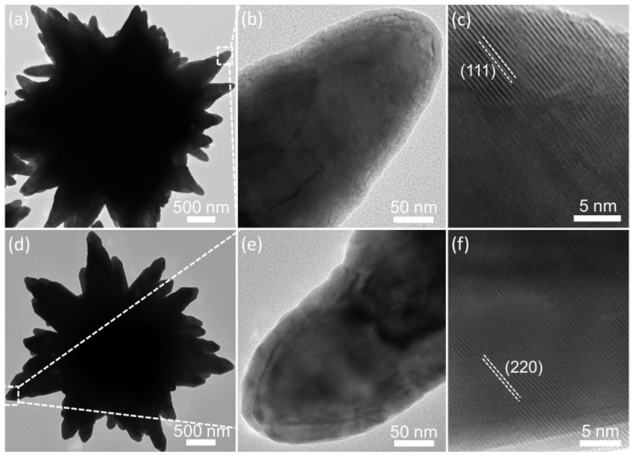

Fig. 3 TEM and HRTEM images of (a)–(c) ZnO@500-Fe_3O_4 and (d)–(f) ZnO@1000-Fe_3O_4.

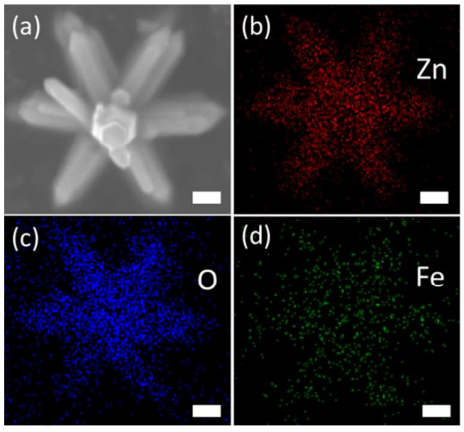

Fig .4 (a) SEM of the ZnO@500-Fe_3O_4 and corresponding elemental mapping images of (b) Zn, (c) O and (d) Fe. Scale bar: 400 nm.

The phase composition and structure of the as-synthesized products are also investigated by XRD analysis. Fig. 5a presents the XRD patterns of ZnO, ZnO@500-Fe_3O_4 and ZnO@1000-Fe_3O_4 products. All of the strong reflection peaks can be readily indexed to those of the hexagonal phase of zincite with the lattice parameters of a = 3.242 Å and c = 5.176 Å, which are consistent with the reported values (Joint Committee on Powder Diffraction Standards (JCPDS), powder diffraction file no. 01-1136). Due to the low content of Fe_3O_4 (Fig. S1), only two relatively weak peaks at 2θ = 43.0° and 53.5° associated with the planes (400) and (422) of the face-centered cubic crystal structure of Fe_3O_4 (JCPDS card 01-1111) for the ZnO@500-Fe_3O_4 and ZnO@1000-Fe_3O_4 are found from the enlarged XRD pattern (Fig. 5b and c). The XRD analysis is in good agreement with both the HRTEM and EDS results.

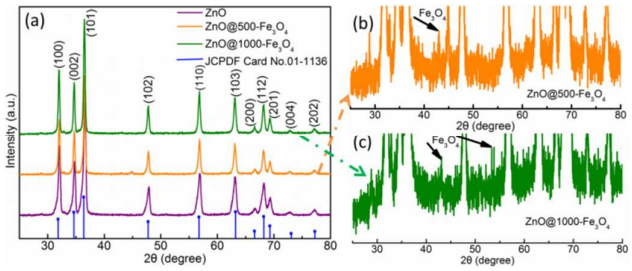

Fig. 5 XRD patterns of ZnO and ZnO@ Fe_3O_4 composites.

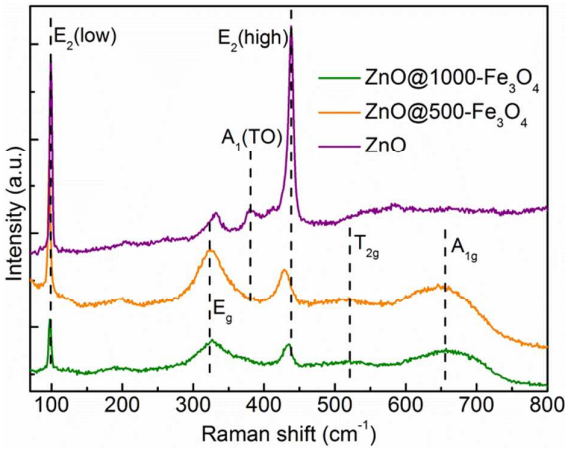

Fig. 6 Raman spectra of ZnO and ZnO@ Fe_3O_4 composites.

We also employed Raman spectroscopy to further characterize the surface functionalities of the samples qualitatively. Fig. 6 shows the Raman spectra of ZnO@Fe_3O_4 by comparison to that of pristine ZnO. For ZnO, two dominant Raman bands at 99 and 655 cm^{-1} are observed, which correspond to the *E_2 (low)* and *E_2 (high)* mode, indicating that the product has perfect crystallinity. The slightly weak peak at 384 cm^{-1} can be attributed to *A_1 (TO)* mode. For ZnO@Fe_3O_4, the weaken *E_2 (low)* and *E_2 (high)* mode imply that the thin layer of Fe_3O_4 shell possibly exists on the surface of the ZnO, as Raman is more sensitive to the sample surface. As shown in Fig. 6, Three fundamental Raman scattering peaks for Fe_3O_4 are observed

at 315, 512, and 663 cm^{-1} corresponding to the E_g, T_{2g}, and A_{1g} vibration modes, respectively.[36] The Raman scattering result unambiguously confirms that the as-prepared core-shell structures observed in the TEM measurements are ZnO@Fe_3O_4, which is consistent with the XRD results.

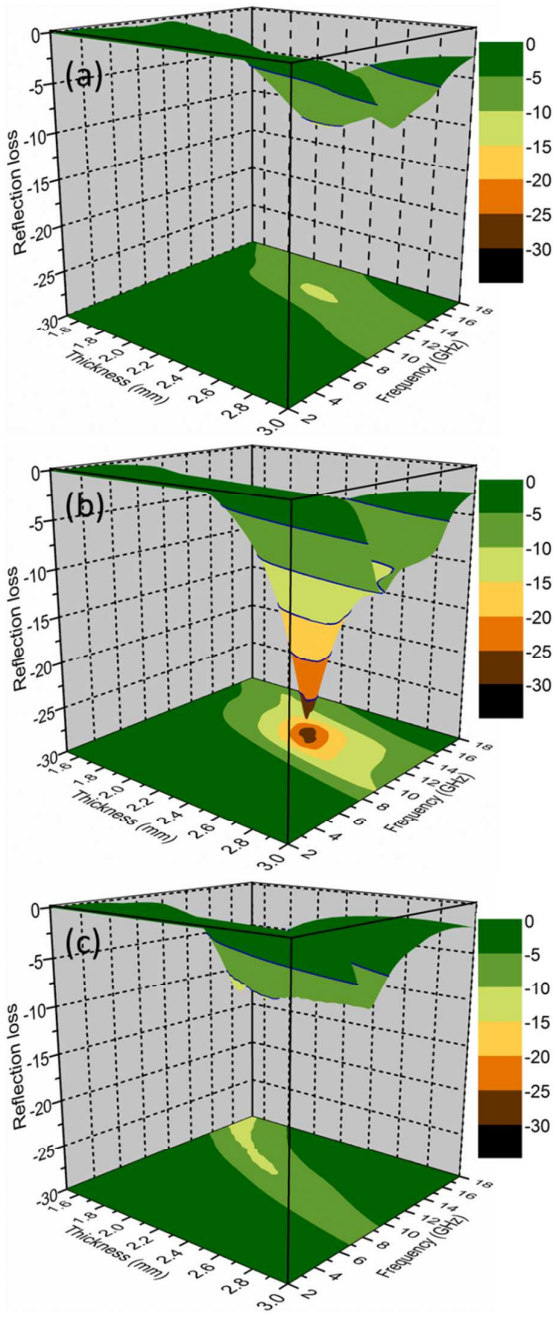

Fig. 7 Three-dimensional representations of the reflection losses of (a) ZnO, (b) ZnO@500-Fe_3O_4 and (c) ZnO@1000-Fe_3O_4.

The reflection loss (RL) coefficients of composite materials by mixing 60 wt% of the samples with paraffin were calculated by using the measured relative complex permittivity and permeability values. According to transmission line theory, the RL coefficient (dB) of electromagnetic wave (normal incidence) at the surface of a single-layer material backed by a perfect conductor at a given frequency and layer thickness can be expressed by the following equations:[37-39]

$$Z_{in} = Z_0(\mu_r/\varepsilon_r)^{1/2}\tanh[j(2\pi fd/c)(\mu_r\varepsilon_r)^{1/2}] \quad (1)$$

$$\mathrm{RL} = 20\log\left|(Z_{in} - Z_0)/(Z_{in} + Z_0)\right| \quad (2)$$

where Z_{in} is the input impedance of the absorber, Z_0 the impedance of free space, ε_r the relative complex permittivity, μ_r the complex permeability, f the frequency of microwaves, d the thickness of the absorber, and c the velocity of light. A RL value of −10 dB is comparable to 90% microwave absorption. In general, materials with RL values of less than −10 dB absorption are considered as suitable EM wave absorbers.

Fig. 7 shows the three-dimensional RL values of ZnO–paraffin and ZnO@Fe_3O_4–paraffin composites with different thicknesses (1.5–3.0 mm) in the frequency range of 2–18 GHz. Pristine ZnO exhibits poor RL characteristics, hardly less than –10 dB which means 90% absorption efficiency in the range of 1.5–3.0 mm. For ZnO@500-Fe_3O_4, the absorption bandwidth for RL values below –10 dB is in the range of 12.5–16.6 GHz with a thickness of only 2.0 mm, corresponding to a bandwidth of 4.1 GHz. When the thickness is 2.3 mm, the sample achieves the best microwave absorption performance. The effective absorption bandwidth below –10 dB can reach 5.2 GHz (10.3–15.5 GHz) and the RL values below –20 dB (99% absorption) also cover a wide frequency range 11.6–14.2 GHz. Moreover, the minimum RL value reaches –28.6 dB at 13.1 GHz. Obviously, the microwave absorption properties ZnO@500-Fe_3O_4 are substantially enhanced relative to the pristine ZnO. Compared with ZnO-based absorption materials reported recently,[27,29,31–33,40] the present ZnO@500-Fe_3O_4 also has a broader bandwidth with a smaller coating thickness. For ZnO@1000-Fe_3O_4, although the minimum RL value is merely –13.0 dB at 16.8 GHz, the microwave absorption values less than –10 dB is obtained in the range of 15.5–18.0 GHz with a thickness of only 1.5 mm.

It is widely accepted that the dielectric loss and magnetic loss are normally responsible for energy attenuation in microwave absorbing coatings. The RL behaviors of materials are usually associated with the relative complex permittivity ($\varepsilon_r = \varepsilon' + i\varepsilon''$) and permeability ($\mu_r = \mu' + i\mu''$) determined by their nature, size and microstructure. As shown in Fig. 8, the μ_r and ε_r of the ZnO–paraffin and ZnO@Fe_3O_4–paraffin composites were evaluated at 2–18 GHz in order to study the possible absorption mechanism. It can be seen that the ε' values of ZnO@Fe_3O_4–paraffin composites increase with the increased thickness of Fe_3O_4 layer (Fig. 8a), which is higher than that of ZnO–paraffin composites. Both ZnO and ZnO@1000-Fe_3O_4 display the slow decline of ε' values in the whole frequency range of 2–18 GHz, while the ε' value of ZnO@500-Fe_3O_4 keeps to 7.8 from 2.0 to 10.3 GHz, then decreases to 5.2 at 14.6 GHz, and increases to

6.6 at 18.0 GHz. As shown in Fig. 8b, it can be noted that the ε'' value remains almost constant (1.20–1.44) in the range of 2–18 GHz for the ZnO–paraffin composites. Whereas, the ε'' value of ZnO@500-Fe_3O_4 increases from 0.6 to 3.0 in the range of 2.0–12.2 GHz, then exhibits a rapid decrease at high frequency. For the ZnO@1000-Fe_3O_4, the ε'' value evidently increases continuously with the increased frequency at 2–18 GHz.

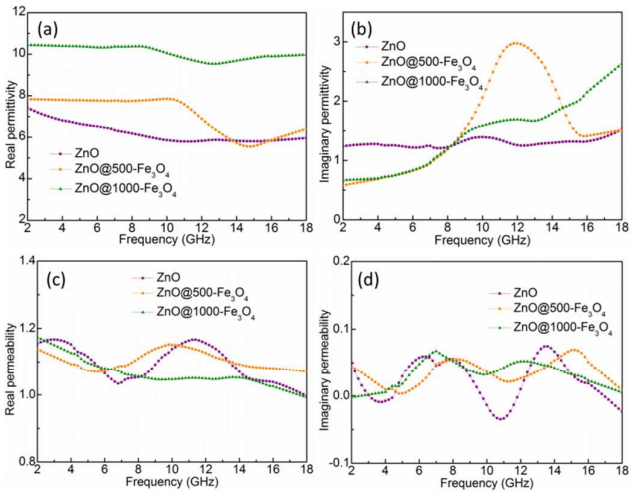

Fig. 8 Measured frequency dependence of (a) real and (b) imaginary parts of complex permittivity and (c) real and (d) imaginary parts of permeability.

Fig.8c and d show the frequency dependence of the measured μ' and μ'' values of the ZnO–paraffin and ZnO@Fe_3O_4–paraffin composites. Owing to only 3.6 wt% and 5.8 wt% of Fe_3O_4 contained in ZnO@500-Fe_3O_4 and ZnO@1000-Fe_3O_4 samples (measured by AAS), the μ' and μ'' of three samples are all about 1.0 and 0.0, respectively. Therefore, the coating of Fe_3O_4 mainly induces the improvement of the response of the electrical component in the microwave frequency band.

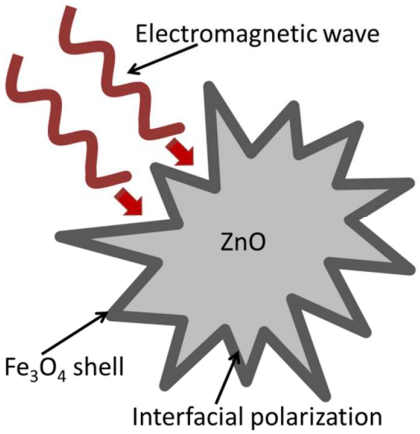

Scheme 1 Schematic representation of the interfacial polarization for the ZnO@Fe_3O_4.

It is known that the ε′ and ε″ of the complex permittivity correspond to the energy storage and attenuation capability, respectively. The ZnO@500-Fe_3O_4 shows higher ε' and ε'' values, suggesting that ZnO@500-Fe_3O_4 has much higher efficiency in storing and attenuating the electrical energy. We calculated the dielectric loss tangent (tan $\delta_E = \varepsilon''/\varepsilon'$) of all the composites, in which the maximum values of tan δ_E are 0.26, 0.45 and 0.27 for ZnO, ZnO@500-Fe_3O_4 and ZnO@1000-Fe_3O_4, respectively (Fig. S2). The larger tan δ_E values for the ZnO@500-Fe_3O_4 and ZnO@1000-Fe_3O_4 imply that the coating of Fe_3O_4 on the surface of ZnO is an efficient strategy to improve the dielectric loss. Dielectric polarizations are mainly composed of the electron polarization, the ion polarization, and the electric dipolar polarization. The electron polarization and ion polarization usually occur at the higher frequency than the infrared frequency. The electric dipolar polarization is well-known dielectric loss mechanism normally responsible for EM wave absorption in the microwave region and might aroused from a heterogeneous interface. Usually, interfacial polarization occurs whenever there is a buildup of a charge at a boundary between two regions or materials.[15,17,41,42] Therefore, the microwave absorption enhancement in present work should be originated from intensified polarization of the ZnO@Fe_3O_4 core-shell interfaces and the proper Fe_3O_4 shell thickness plays an important role to maximize the interface effect. Debye dipolar relaxation is utilized to further understand absorbing mechanisms of the ZnO and ZnO@Fe_3O_4. Only an obvious Cole–Cole semicircle (Fig. S3) is found for the ZnO@500-Fe_3O_4 among three samples, which reconfirms that there is the relative intense dielectric relaxation process probably ascribed to the interface polarization. To further give a visual demonstration of the microwave absorption mechanism of ZnO@Fe_3O_4 composites as discussed above, a schematic is given in Scheme 1.

Conclusions

In summary, ZnO@Fe_3O_4 core-shell structures with controllable shell thickness were successfully synthesized through an atomic layer deposition method. The as-prepared ZnO@Fe_3O_4 composites with proper Fe_3O_4 coating show excellent microwave absorption performances included the broad bandwidth and the small coating thickness. The enhanced microwave absorption properties are attributed to the increased relatively complex permittivity and the promoted dielectric loss by the intense interfacial dielectric polarizations.

Acknowledgements

This work was supported by the National Natural Science Foundation of China (11564011, 51362010), the Natural Science Foundation of Hainan Province (514207, 514212), the Scientific Research Projects of Colleges and Universities of Hainan Province (HNKY2014-14), and the Scientific Research Projects of Hainan University (kyqd1502).

Notes and references

1 B. Wen, M. Cao, M. Lu, W. Cao, H. Shi, J. Liu, X. Wang, H. Jin, X. Fang, W. Wang and J. Yuan, *Adv. Mater.*, 2014, **26**, 3484.
2 L. Kong, Z. Li, L. Liu, R. Huang, M. Abshinova, Z. Yang, C. Tang, P. Tan, C. Deng and S. Matitsine, *Int. Mater. Rev.*, 2013, **58**, 203.
3 Y. Zhang, Y. Huang, T. Zhang, H. Chang, P. Xiao, H. Chen, Z. Huang and Y. Chen, *Adv. Mater.*, 2015, **27**, 2049.
4 M.-S. Cao, X.-X. Wang, W.-Q. Cao and J. Yuan, *J. Mater. Chem. C*, 2015, **3**, 6589.
5 G. Wang, Z. Gao, S. Tang, C. Chen, F. Duan, S. Zhao, S. Lin, Y. Feng, L. Zhou and Y. Qin, *ACS Nano*, 2012, **6**, 11009.
6 X. Zhang, J. Guo and G. Qin, *Appl. Phys. Lett.*, 2014, **104**, 252404.
7 G.-S. Wang, X.-J. Zhang, Y.-Z. Wei, S. He, L. Guo and M.-S. Cao, *J. Mater. Chem. A*, 2013, **1**, 7031.
8 X. Liu, B. Li, D. Geng, W. Cui, F. Yang, Z. Xie, D. Kang and Z. Zhang, *Carbon*, 2009, **47**, 470.
9 G. Sun, B. Dong, M. Cao, B. Wei and C. Hu, *Chem. Mater.*, 2011, **23**, 1587.
10 Z. An, J. Zhang and S. Pan, *Dalton Trans.*, 2010, **39**, 3378.
11 Y.-Z. Wei, G.-S. Wang, Y. Wu, Y.-H. Yue, J.-T. Wu, C. Lu and L. Guo, *J. Mater. Chem. A*, 2014, **2**, 5516.
12 N. N. Song, Y. J. Ke, H. T. Yang, H. Zhang, X. Q. Zhang, B. G. Shen and Z. H. Cheng, *Sci. Rep.*, 2013, **3**, 2291.
13 H.-C. Yu, L.-C. Hsu, T.-H. Chang and Y.-Y. Li, *Dalton Trans.*, 2012, **41**, 723.
14 G. Wang, Z. Gao, G. Wan, S. Lin, P. Yang and Y. Qin, *Nano Res.*, 2014, **7**, 704.
15 T. Xia, C. Zhang, N. A. Oyler and X. Chen, *Adv. Mater.*, 2013, **25**, 6905.
16 H. Sun, R. Che, X. You, Y. Jiang, Z. Yang, J. Deng, L. Qiu and H. Peng, *Adv. Mater.*, 2014, **26**, 8120.
17 J. Liu, R. Che, H. Chen, F. Zhang, F. Xia, Q. Wu and M. Wang, *Small*, 2012, **8**, 1214.
18 X. Liu, Z. Ou, D. Geng, Z. Han, J. Jiang, W. Liu and Z. Zhang, *Carbon*, 2010, **48**, 891.
19 X. Liu, D. Geng, H. Meng, P. Shang and Z. Zhang, *Appl. Phys. Lett.*, 2008, **92**, 173117.
20 X. Zhang, Y. Liu and G. Qin, *Appl. Phys. Lett.*, 2015, **106**, 033105.
21 H. Wang, L. Wu, J. Jiao, J. Zhou, Y. Xu, H. Zhang, Z. Jiang, B. Shen and Z. Wang, *J. Mater. Chem. A*, 2015, **3**, 6517.
22 C. Liu, Y. Xu, L. Wu, Z. Jiang, B. Shen and Z. Wang, *J. Mater. Chem. A*, 2015, **3**, 10566.
23 J. Dong, R. Ullal, J. Han, S. Wei, X. Ouyang, J. Dong and W. Gao, *J. Mater. Chem. A*, 2015, **3**, 5285.
24 K. Yuan, R. Che, Q. Cao, Z. Sun, Q. Yue and Y. Deng, *ACS Appl. Mat. Interfaces*, 2015, **7**, 5312.
25 X. Zhang, G. Ji, W. Liu, B. Quan, X. Liang, C. Shang, Y. Cheng and Y. Du, *Nanoscale*, 2015, **7**, 12932.
26 J. Liu, W.-Q. Cao, H.-B. Jin, J. Yuan, D.-Q. Zhang and M.-S. Cao, *J. Mater. Chem. C*, 2015, **3**, 4670.
27 Q. Hu, G. Tong, W. Wu, F. Liu, H. Qian and D. Hong, *CrystEngComm*, 2013, **15**, 1314.
28 R. Zhuo, H. Feng, J. Chen, D. Yan, J. Feng, H. Li, B. Geng, S. Cheng, X. Xu and P. Yan, *J. Phys. Chem. C*, 2008, **112**, 11767.
29 R. Zhuo, L. Qiao, H. Feng, J. Chen, D. Yan, Z. Wu and P. Yan, *J. Appl. Phys.*, 2008, **104**, 094101.
30 H. Lv, G. Ji, M. Wang, C. Shang, H. Zhang and Y. Du, *RSC Adv.*, 2014, **4**, 57529.
31 L. Zhang, X. Zhang, G. Zhang, Z. Zhang, S. Liu, P. Li, Q. Liao, Y. Zhao and Y. Zhang, *RSC Adv.*, 2015, **5**, 10197.
32 G. Wang, X. Peng, L. Yu, G. Wan, S. Lin and Y. Qin, *J. Mater. Chem. A*, 2015, **3**, 2734.
33 J. Cao, W. Fu, H. Yang, Q. Yu, Y. Zhang, S. Liu, P. Sun, X. Zhou, Y. Leng and S. Wang, *J. Phys. Chem. B*, 2009, **113**, 4642.
34 G.-S. Wang, Y.-Y. Wu, X.-J. Zhang, Y. Li, L. Guo and M.-S. Cao, *J. Mater. Chem. A*, 2014, **2**, 8644.
35 M.-M. Lu, W.-Q. Cao, H.-L. Shi, X.-Y. Fang, J. Yang, Z.-L. Hou, H.-B. Jin, W.-Z. Wang, J. Yuan and M.-S. Cao, *J. Mater. Chem. A*, 2014, **2**, 10540.
36 D. De Faria, S. Venâncio Silva and M. De Oliveira, *J. Raman Spectrosc.*, 1997, **28**, 873.
37 R. Che, L. M. Peng, X. F. Duan, Q. Chen and X. Liang, *Adv. Mater.*, 2004, **16**, 401.
38 H. Lv, G. Ji, X. Liang, H. Zhang and Y. Du, *J. Mater. Chem. C*, 2015, **3**, 5056.
39 T. Xia, Y. Cao, N. A. Oyler, J. B. Murowchick, L. Liu, X. Chen, *ACS Appl. Mat. Interfaces*, 2015, **7**, 10407.
40 X. Liu, D. Geng, P. Shang, H. Meng, F. Yang, B. Li, D. Kang and Z. Zhang, *J. Phys. D: Appl. Phys.*, 2008, **41**, 175006.
41 G. Wan, L. Yu, X. Peng, G. Wang, X. Huang, H. Zhao and Y. Qin, *RSC Adv.*, 2015, **5**, 77443.
42 B. Zhao, B. Fan, G. Shao, W. Zhao and R. Zhang, *ACS Appl. Mater. Interfaces*, 2015, **7**, 18815.

TOC

Uniform ZnO@Fe_3O_4 core–shell structure is prepared by an ALD method, which shows great potential for microwave absorption materials.